Nat. Hazards Earth Syst. Sci., 14, 11–20, 2014
www.nat-hazards-earth-syst-sci.net/14/11/2014/
doi:10.5194/nhess-14-11-2014

Natural Hazards and Earth System Sciences
Open Access

Numerical modeling of the lateral widening of levee breach by overtopping in a flume with 180° bend

S.-T. Dou[1,2], D.-W. Wang[3], M.-H. Yu[4], and Y.-J. Liang[5]

[1]Cold and Arid Regions Environmental and Engineering Research Institute, Chinese Academy of Sciences, 73000 Lanzhou, China
[2]Yellow River Institute of Hydraulic Research, YRCC, 450003 Zhengzhou, China
[3]State Key Laboratory of Simulation and Regulation of River Basin Water Cycle, China Institute of Water Resources and Hydropower Research, 100038 Beijing, China
[4]State Key Laboratory of Water Resources and Hydropower Engineering Sciences, Wuhan University, 430072 Wuhan, China
[5]Yellow River Engineering Consulting Co., Ltd. YRCC, Zhengzhou, 450003, China

Correspondence to: D.-W. Wang (wangdw17@126.com)

Received: 3 July 2013 – Published in Nat. Hazards Earth Syst. Sci. Discuss.: 8 August 2013
Revised: 26 November 2013 – Accepted: 28 November 2013 – Published: 3 January 2014

Abstract. Floods caused by levee breaching pose disastrous risks to the lower reaches and the flood flow zones of rivers. Thus, a comprehensive assessment of flow and sediment transport during floods must be performed to mitigate flood disasters. Given that the flow state becomes relatively more complex and the range of the submerged area becomes more extensive after a levee breach, this paper established a flow and sediment model by using two-dimensional shallow water equations (SWEs) to explore the breach development process and the flow and sediment transport in a curved bed after a levee breach due to overtopping. A three-element weighted essentially non-oscillatory Roe scheme was adopted for the discretization of SWEs. In addition, a non-equilibrium total-load sediment transport model was established to simulate the scour depth development process of the breach. A stable equilibrium of the breach was established based on flow shear force and soil shear strength. The lateral widening of the breach was simulated by the scouring-collapse lateral widening mode. These simulations, together with the levee breach experiment conducted in the laboratory, demonstrate the validity of the flow and sediment transport process established in this paper. The effects of water head in and out of the watercourse, the flow rate, the levee sediment grading, and other variables during levee breaching were also analyzed. The mathematical model calculation provided a number of physical quantities, such as flow rate and flow state at the breach, that are difficult to measure by using the current laboratory facilities. The results of this research provide fundamental data for developing measures that can reduce casualties and asset loss due to floods caused by levee breaching.

1 Introduction

Floods caused by levee breaching due to overtopping can cause major disasters. Thus, many scholars have indicated the importance of studying this area. To date, a considerable number of fruitful studies have been conducted (Morris, 2009). Risk assessment is a crucial premise for the mitigation of flood disasters. However, the flood development process, which is crucial to flood from levee breaching, must first be understood before flood risk assessment can be conducted (Apel et al., 2006). The use of mathematical models to calculate flood from levee breaching is currently a focus of several studies (Wu and Wang, 2007, Wu et al., 2012; Yu et al., 2009; Savant 5 et al., 2010; Liu and Wu, 2011; Chen, 2013).

In levee breach calculations, changes in details, such as local flow through breach, topographical changes, and mouth lateral widening velocity, should be accurately recorded. Thus, the mathematical model of a levee breach requires an accurate flow calculation and a precise simulation of breach development. Most existing studies consider dikes or levees

as homogeneous materials. The development of break can generally occur in two ways: instant collapse and progressive collapse. For an instant collapse, the break is assumed to have formed instantly, and the form of break is difficult to change. The numerical simulation of concrete levees or stonemason levees can only handle simpler situations. However, in reality, a progressive collapse is the more frequent cause of levee breaching. Thus, if the lateral widening of the breach is ignored, and the instant collapse of the earth dike is assumed, then more significant errors will be generated. However, given the complexity of the problem, researchers generally provide assumptions for the breach position and shape when developing simulations. If the initial shape of the breach is more regular and the section in its development process is uniformly eroded, then the initial shape is maintained. For example, if the initial break is triangular, rectangular, trapezoidal, or parabolic, the shape is maintained, and only the enhanced breaching or depth is shown. Cristofano (1973) established the first numerical simulation of progressive erosion and earth-rockfill levee breaching. The width of the break with trapezoidal shape remained unchanged in the model. In addition, only the vertical erosion and scouring were considered, and the maximal scouring reached only the bedrock. The scouring of the side slope was not considered. The lateral widening of the levee started from the vertical erosion and scouring to the side slope collapse. In contrast to the sediment amount in the flow, the sediment amount from the side slope collapse can be neglected. The fluted bed slope was equal to the internal friction angle of earth fills. Harris and Wagner (1967) executed the following modifications on the model developed by Cristofano: the top width was 3.75 times the length of the depth, the side slope had a parabolic form of approximately 45°, and the erosion of the break was assumed to develop at the bottom of the dam. During the 1980s, Lou (1981) proposed a mathematical model of a progressive collapse of an earth-rock dam caused by overtopping. The most distinctive feature of this model was that the breach form was not assumed without previous notice, and the analytical solution of the breach form was deducted from the shear stress and the erosion mechanism. Nogueira (1984) also presented a model similar to Lou's. The most significant difference between the two models was the means of identifying the break shape. In the model by Nogueira, the shape of the transverse section of the fluted breach was identified by the effective shear stress, that is, the difference between the total shear stress at a point and the critical shear stress. In 1984, Fread (1984) successfully developed the DAMBRK model, which required fewer parameters to identify the break shape. In this model, the initial break shape can be identified with a single parameter. The break shape, including the rectangular, triangular, and trapezoidal shapes, can be identified by adjusting this single parameter. The ultimate break size was determined by the final bottom width of the break. However, the specific calculation of sediment transportation was not included in this model. The breach development process was assumed to evolve with linear velocity over time. In the subsequent BREACH model developed by Fread (1988), the identification method of the breach shape and the breach development process were improved. Fread provided two methods for further application. The first method assumed the initial breach shape as a rectangle, whereas the other method involved the deduction of the breach width on the basis of slope stability. A collapse happens when the undercut depth of the breach reaches the critical depth. The critical depth depends on the internal friction angle, the cohesive force, the angle formed by the lateral and horizontal directions of the breach, and the density of the levee materials. Faeh (2007) adopted the 2D flow and sediment model to simulate the flow rate of the break in levee breaching due to overtopping and assessed the effect of each parameter on the flow rate of the breach. Wu et al. (2012) applied the Harten, Lax and van Leer (HLL) Riemann solver with second-order accuracy to simulate the levee breaching process of a non-cohesive soil embankment.

These various levee breach models primarily propose three assumptions: (1) the break shape remains unchanged; (2) the breach section in the breach development was scoured homogeneously; (3) the materials of the levee were homogeneous. These assumptions have slight inconsistencies with reality, which reduces the reliability of the calculation results. Instead of these assumptions, an approach for calculating flow and sediment movement in levee breach based on hydrodynamics and morphodynamics is proposed in this paper. The aim of this study is to test the applicability of this approach for simulation of levee breach processes, and this was done by establishing a non-equilibrium total-load sediment transport model and the scouring-collapse mode of breach lateral widening based on the high-precision numerical format in calculating the flow from levee breaching to simulate the scour depth and lateral widening of breach development. In addition, levee breaching experiments were conducted, and the results verified the capability of this method to calculate the flow and sediment transport of the levee breach. The effects of parameters, including water head in and out of the course, the flow rate, and levee sediment grading during levee breaching were analyzed. A number of physical quantities that are difficult to measure using the existing experimental methods, such as the flow rate at the break and the flow regime, were supplemented. In view of these results, the methodology developed in this paper seems to be useful for modeling and predicting earth levee breach processes caused by overtopping, which is helpful in preventing and controlling flood disaster.

2 Methods

2.1 WENO–Roe method for shallow water equation

The diffusion term can be ignored in the SWEs because of the specific characteristics of levee breach flow and the dominant

role of the convection. Thus, to consider the drastically topographic changes in the levee breaching process and the enormous sediment concentration in the flow, the fundamental equation adopted the conservation form (Toro, 2001)

$$\frac{\partial \boldsymbol{U}}{\partial t}+\frac{\partial \boldsymbol{F}}{\partial x}+\frac{\partial \boldsymbol{G}}{\partial y}=\boldsymbol{S}(\boldsymbol{U}), \tag{1}$$

where

$$\boldsymbol{U}=\begin{bmatrix}\rho h\\ \rho hu\\ \rho hv\end{bmatrix};\boldsymbol{F}=\begin{bmatrix}\rho hu\\ \rho hu^2+\frac{1}{2}\rho gh^2\\ \rho huv\end{bmatrix};$$
$$\boldsymbol{G}=\begin{bmatrix}\rho hv\\ \rho huv\\ \rho hv^2+\frac{1}{2}\rho gh^2\end{bmatrix};\boldsymbol{S}=-\begin{bmatrix}\rho_{\mathrm{b}}\frac{\partial z_{\mathrm{b}}}{\partial t}\\ gh\left(s_x-f_x-\frac{1}{2}h\frac{\partial \rho}{\partial x}\right)\\ gh\left(s_y-f_y-\frac{1}{2}h\frac{\partial \rho}{\partial y}\right)\end{bmatrix};$$

t represents time; x and y represent the longitudinal and the lateral coordinates, respectively; h represents the flow depth; u and v represent the flow velocities along the x and y directions, respectively; $\partial z_{\mathrm{b}}/\partial t$ represents the rate of change in bed surface elevation; z_{b} represents the bed surface elevation above the reference datum; g represents the gravitational acceleration; ρ represents the density of the water and sediment mixture in the water column determined by $\rho=\rho_{\mathrm{w}}(1-S_{\mathrm{t}})+\rho_{\mathrm{s}}S_{\mathrm{t}}$. Here, S_{t} represents the volumetric concentration of the total-load sediment; ρ_{w} and ρ_{s} represent the water and the sediment densities, respectively. ρ_{b} represents the density of the water and the sediment mixture on the bed surface layer determined by $\rho_{\mathrm{b}}=\rho_{\mathrm{w}}p_{\mathrm{m}}+\rho_{\mathrm{s}}(1-p_{\mathrm{m}})$, in which p_{m} represents the porosity of the surface-layer bed material. s_x and s_y represent the bed slopes along the x and y directions, respectively, which are determined by $s_x=-\frac{\partial z_{\mathrm{b}}}{\partial x}$–$s_y=-\frac{\partial z_{\mathrm{b}}}{\partial y}$. f_x and f_y represent the bed friction due to bed roughness along the x and y directions, respectively, which can be estimated by empirical formulation as $f_x=\frac{n^2u\sqrt{u^2+v^2}}{h^{4/3}}$and $f_y=\frac{n^2v\sqrt{u^2+v^2}}{h^{4/3}}$. n represents the Manning roughness coefficient; $m_{\mathrm{b}}=\sqrt{1+\left(\frac{\partial z_{\mathrm{b}}}{\partial x}\right)^2+\left(\frac{\partial z_{\mathrm{b}}}{\partial y}\right)^2}$ is considered the curved bed (bank) surface or perimeter.

On the basis of the Godunov discretization pattern in the conservation equation, the control Eq. (1) can be discretized into (Toro, 2001):

$$\boldsymbol{U}_{i,j}^{n+1}=\boldsymbol{U}_{i,j}^{n}-\frac{\Delta t}{\Delta x}\left(\boldsymbol{F}_{i+\frac{1}{2},j}^{*}-\boldsymbol{F}_{i-\frac{1}{2},j}^{*}\right)-\frac{\Delta t}{\Delta x}\left(\boldsymbol{G}_{i,j+\frac{1}{2}}^{*}-\boldsymbol{G}_{i,j-\frac{1}{2}}^{*}\right)-\Delta t\boldsymbol{S}, \tag{2}$$

where $\boldsymbol{F}_{i\pm\frac{1}{2},j}^{*}$ and $\boldsymbol{G}_{i,j\pm\frac{1}{2}}^{*}$ represent the flux value at the interface formed by the x and y directions, respectively; Δt is the time step; Δx and Δy represent the spatial step along the x and y directions, respectively. The grid is shown in Fig. 1.

Equation (2) can be solved by accurately building the numerical flux of the interface as $\boldsymbol{F}_{i\pm\frac{1}{2},j}^{*}$, $\boldsymbol{G}_{i,j\pm\frac{1}{2}}^{*}$, from which

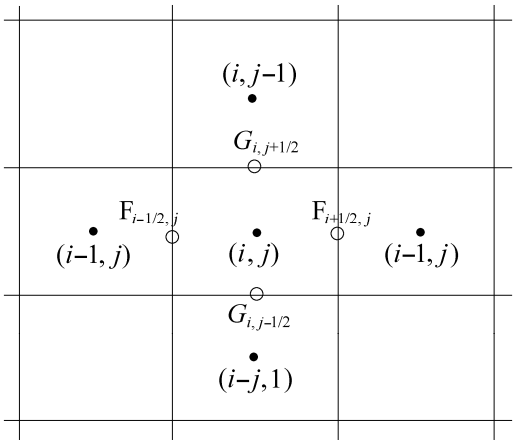

Fig. 1. Solution grid.

high-precision conserved variables can be established. In order to make the result more accurate, the WENO–Roe approach is used to calculate the numerical flux. The WENO scheme (Shu, 2003) is adopted to solve for the values of the conservation variables on both sides of the unit interface to obtain the numerical flux at the interface. First, the unit number contained by the template must be identified because high resolution and high precision can be achieved by increasing the unit number in the template. Given the complexity of the computation, a three-unit template, which can reach the fifth order, was used. Thus, the weight coefficient w_{r} can be expressed as (Shu, 2003)

$$w_{\mathrm{r}}=\frac{\alpha_{\mathrm{r}}}{\sum_{s=0}^{k-1}\alpha_{\mathrm{s}}}--r=0,\cdots,k-1,\alpha_{\mathrm{r}}=\frac{d_{\mathrm{r}}}{(\varepsilon+\beta_{\mathrm{r}})^2}, \tag{3}$$

where β_{r} is the smooth factor; $\varepsilon>0$ and a minimal value is generally obtained to prevent the denominator from becoming zero. In this paper, the value of ε was 10^{-6}.

The difficulty in numerically solving the Riemann discontinuous decomposition is caused by the complexity of the discontinuous decomposition generated by nonlinearity. The Roe method was used to apply the conservation variable of the adjacent constant states to derive a rational linear matrix that can replace the complex nonlinear matrix. In this way, the complex nonlinear issue was transformed into a linear issue. After linearization, the characteristics of the numerical flux can be presented as (Roe, 1981)

$$\boldsymbol{F}_{i+\frac{1}{2},j}^{*}=\frac{1}{2}\left(\boldsymbol{F}_{i+\frac{1}{2},j}(\boldsymbol{U}_{\mathrm{l}})+\boldsymbol{F}_{i+\frac{1}{2},j}(\boldsymbol{U}_{\mathrm{r}})-\sum_{k=1}^{3}\tilde{\alpha}_k|\lambda_k|\tilde{\boldsymbol{e}}_k\right). \tag{4}$$

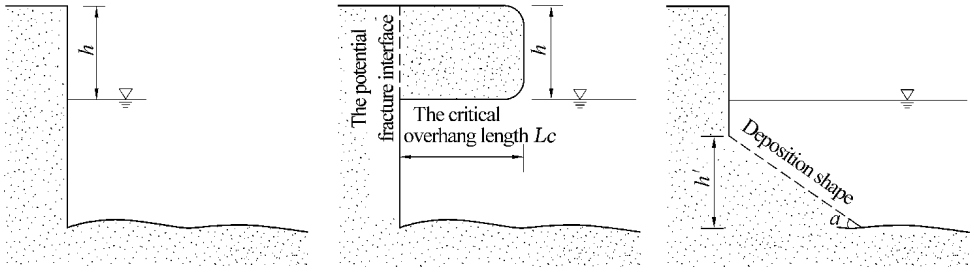

Fig. 2. Lateral widening mode of the break.

On the basis of the principles mentioned above, each feature quantity can be obtained from Eq. (4) as follows:

$$\alpha_1 = \frac{1}{2c}\left[\Delta(hu) - (\tilde{u} - c)\,\Delta h\right],$$
$$\alpha_2 = \frac{1}{c}\left[\Delta(hv) - \tilde{v}\Delta h\right],$$
$$\alpha_3 = \frac{1}{2c}\left[(\tilde{u} + c)\,\Delta h - \Delta(hu)\right];$$

$$\lambda_1 = \tilde{u} + c, \quad \lambda_2 = \tilde{u}, \quad \lambda_3 = \tilde{u} - c;$$
$$\boldsymbol{e}_1 = \left[1\tilde{u} + cv\right], \boldsymbol{e}_2 = [00c], \quad \boldsymbol{e}_3 = \left[1\tilde{u} - cv\right],$$

where $\tilde{u} = \frac{\sqrt{h_\mathrm{r}}u_\mathrm{r} + \sqrt{h_\mathrm{l}}u_\mathrm{l}}{\sqrt{h_\mathrm{l}} + \sqrt{h_\mathrm{r}}}$, $\tilde{v} = \frac{\sqrt{h_\mathrm{r}}v_\mathrm{r} + \sqrt{h_\mathrm{l}}v_\mathrm{l}}{\sqrt{h_\mathrm{l}} + \sqrt{h_\mathrm{r}}}$, and $c = \frac{\sqrt{gh_\mathrm{r}} + \sqrt{gh_\mathrm{l}}}{2}$ are Roe's average, and $\boldsymbol{\Delta U} = \boldsymbol{U}_\mathrm{r} - \boldsymbol{U}_\mathrm{l}$ represents the increase in values of the conservation variables at both sides of the interface. Similarly, the Roe parameter vectors along the y direction can be obtained to form $\boldsymbol{G}^*_{i,j+\frac{1}{2}}$.

The third-order Runge–Kutta TVD method and the slop flux method were adopted to process the source term to ensure the accuracy and the stability of the calculation (Wang et al., 2012).

2.2 Bed scouring and lateral widening of the breach

2.2.1 Bottom scouring simulation

For the bed scouring of the breach, the inhomogeneous and imbalanced sediment transfer mode was used in the calculation, and the basic equations are presented as follows:

Continuity equation of the sediment:

$$\frac{\partial(hS_k)}{\partial t} + \frac{\partial(huS_k)}{\partial x} + \frac{\partial(hvS_k)}{\partial x} + \rho'\frac{\partial z_{\mathrm{bs}k}}{\partial t} = \frac{\partial}{\partial x}\left(D_\mathrm{s}\frac{\partial(hS_k)}{\partial x}\right) + \frac{\partial}{\partial y}\left(D_\mathrm{s}\frac{\partial(hS_k)}{\partial y}\right) \quad (5)$$

Suspended sediment deformation equation:

$$\rho_\mathrm{b}\frac{\partial z_{\mathrm{bs}k}}{\partial t} = \alpha\omega_k\,(S_k - S_{*k}) \quad (6)$$

Bed-load deformation equation:

$$\rho_\mathrm{b}\frac{\partial z_{\mathrm{bg}k}}{\partial t} + \frac{\partial g_{\mathrm{bx}k}}{\partial x} + \frac{\partial g_{\mathrm{by}k}}{\partial y} = 0, \quad (7)$$

where ρ_b represents the dry density of the riverbed sludge; D_s represents the sediment diffusion coefficient; S_k represents the sediment content in the kth group; S_{*k} represents the flow sediment-carrying capacity in the kth group; $z_{\mathrm{bs}k}$ and $z_{\mathrm{bg}k}$ represent the river bed elevation change caused by the movement of the suspended load and the bed load in the kth group, respectively; $g_{\mathrm{bx}k}$ and $g_{\mathrm{by}k}$ represent the transport rate per unit of the bed load along the x and y directions in the kth group, respectively; α represents the saturation recovery coefficient. The discretization of the equation adopted the semi-implicit upwind scheme of discretization (Wang et al., 2007). Thus, the time step of the scour model can be much larger than that of the flow model, which makes the calculation more efficient and stable. In the model whole sediments are set as a single mix layer, and after every time step the composition of this layer will be adjusted according to the amount of sediment carried by flow.

2.2.2 Lateral widening mode of the breach

The collapse-lateral widening mode was adopted to simulate the lateral widening of the breach. Instead of needing the differentiated interface between cohesive soil and non-cohesive soil, the part of the levee under the water was subjected to lateral scouring, whereas the part above the water was subjected to the lateral widening from the suspending collapse. Based on the experiment, a part of the sediments produced from the collapse was removed by the flow. The rest were piled on the bed according to the underwater slope of repose α of flowing water.

Figure 2 shows the generalized lateral mode based on existing research results and experimental observations.

In Δt, the recession distance of the cohesive soil bank caused by the lateral scouring from the flow was

$$\Delta B = \frac{C_\mathrm{l} \times \Delta t \times (\tau - \tau_\mathrm{c})e^{-1.3\tau_\mathrm{c}}}{\gamma_{\mathrm{b}k}}, \quad (8)$$

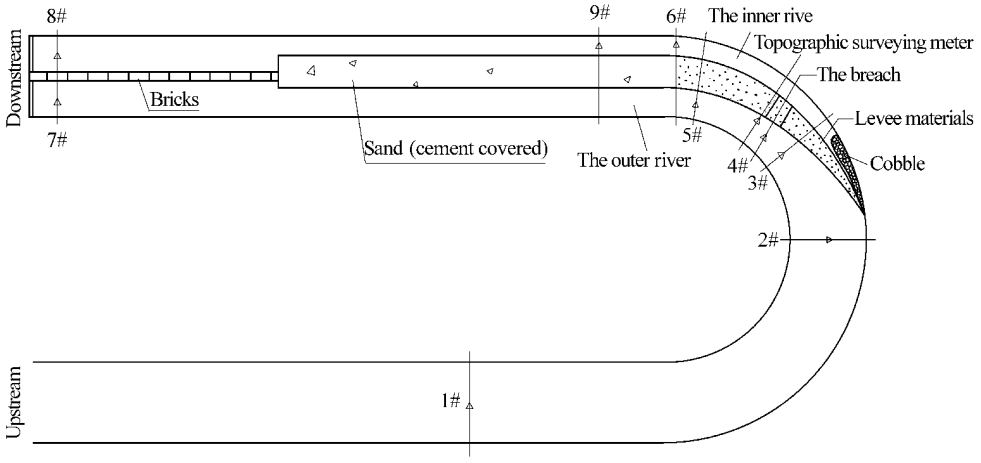

Fig. 3. Sketch of the experiment layout.

where γ_{bk} is the unit weight of riverbank soils (kN m^{-3}); ΔB is the distance of the bank recession from the lateral widening of the flow lateral scouring in Δt(m); τ is the flow shear stress on the bank (N m^{-2}); τ_c is the start-up shear stress of riverbank soils (N m^{-2}); C_l is the coefficient of lateral scouring, which is related to the physical and chemical properties of riverbank soils. According to the test results, $C_l = 3.6 \times 10^{-4}$, which was basically the same as the results proposed by Osman and Thorne (1988).

$$\tau = \gamma \frac{U^2}{C^2} \tag{9}$$

Here, the resultant velocity is $U = \sqrt{u^2 + v^2}$; γ is the bulk density of the water; C is the Chezy coefficient, which can be obtained by the Manning formula.

For τ_c, the critical drag force equation of the Shields coarse sediment was

$$\tau_c = k(\gamma_s - \gamma)d, \tag{10}$$

where k is the coefficient ranging from 0.04 to 0.06, γ_s is sediment bulk density, and d is the sediment particle size.

Given that the lower embankment recessed because of flow scouring, the upper part was suspended (see Fig. 2b). When the stress on the upper part of the fracture interface reached the strength of extension, the applied moment produced by the suspended deadweight W created a balance with the stretching resistance produced by the fracture surface to derive the mechanical equilibrium equation. Thus, the equation of the critical overhang length of the river bank can be expressed as follows:

$$L_c = (T_0 \cdot H/3\gamma_2)^{1/2}, \tag{11}$$

where H, B, γ_2, and T_0 represent the height, the width, the density, and the strength of extension of the soils, respectively.

When $L < L_c$, the cohesive soil layer of the upper part of the riverbank stayed stable and did not collapse. The flow can keep a non-cohesive soil layer.

When $L = L_c$, the cohesive soil layer of the upper part of the riverbank reaches a critical extension value, and a collapse is about to occur.

When $L > L_c$, the cohesive soil layer of the upper part of the riverbank might have collapsed. The critical state of collapsing can be achieved by adjusting the time step.

2.2.3 Introduction of flume experiments

The experiment was conducted in a glass flume of a 180° curved bed (bank). The flume was 1.2 m wide, the bed slope was 1 %, and the radius of the inner curve was 1.8 m. As shown in Fig. 3, a 20 cm-wide rectangle break was created at the 4# section (4# section as axis), the elevation of which is lower than the elevation of both sides of the riverbank by 1.5 cm. In the experiment, this rectangle break was used as the break of the levee breach. When the water level was raised to a certain height, the flow was effused from the induced break, and the levee started to outburst.

A water level meter was set up at each section from the upstream to the downstream of the flume to observe the variation in the water level in and out of the riverbank after the levee breach. A total of nine sets was deployed. Each water level meter was set to record the local water level every 2 s. The sections of the flume were set as follows: 1# at the upstream straight section, 2# at the curve top, 3# at the upstream of the induced break of the outer river, 4# at the induced break of the outer river, 5# at the end of the curve section of the outer river, 6# and 9# at the downstream straight section of the inner river, 7# around the stern door of the outer river, and 8# near the stern door of the inner river to deduct the flow rate in the levee breach. In addition, a graphometer, which can measure the real-time elevation changes in the

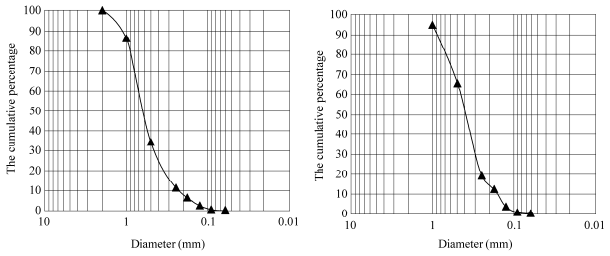

Fig. 4. Coarse sand grading curve.

break, was set in the downstream area of the 4# section of the levee to observe the vertical development process of the breach after levee breaching. The layout chart of the experiment is depicted in Fig. 3.

Inhomogeneous sediments comprising two grading levels were used as levee materials to determine the effect of the levee material on the levee breaching process. The grading curves of the sediments are shown in Figs. 4 and 5. The medium-sized particle among the relatively coarse sediments was approximately 0.6 mm (Fig. 4), whereas that of the refined group was approximately 0.4 mm (Fig. 5).

3 Results

3.1 Changing process of water level

Figure 6 shows that the water level meters at the 4# and 6# sections were set on both sides near the breach. These water level meters recorded the variation in water level during the levee breaching process. The instant levee water head at the breach of the inner and the outer river (4# and 6#) reached a maximal value. The flow of the outer river was rapidly elevated in the inner river, which flowed down from the breach. The water head in and out of the river gradually decreased as the break width gradually expanded. In the levee breach, the water level of the outer river declined steadily, whereas that of the inner river changed drastically, from initially reaching the maximal level to gradually declining to a stable level. The flow state of the breach was complex. Experiments reveal that the turbulent fluctuation of the flows in the breach area became intense. Figure 6 also shows that the water level fluctuation at 6# was intense. The calculation results were generally consistent with the overall experimental results, verifying the feasibility of this numerical simulation.

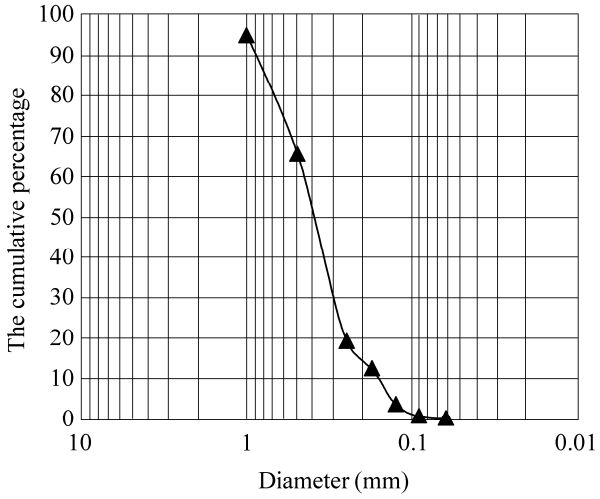

Fig. 5. Fine sand grading curve.

3.2 Flow structure and quantity of breach

The classic flow field near the breach is presented in Fig. 7. Figure 7a shows that at 10 s after the levee breach and overtopping, the flow of the outer river was imported into the inner river at the breach from the outer river. The flow direction was vertical to the breach and was split into two when the flow crushed on the wall of the curved bed (bank). Most of the flows went into the downstream along the curved bed (bank). The bending direction of a few flows was blocked by the wall, forming vortexes. Figure 7b shows that at 50 s, the break flow direction turned to the downstream of the inner river, forming an intersection angle with the breach. As the breach continued to expand, the direction of the flow through the breach changed accordingly, with the intersection angle getting smaller, since the main flow is always near the left side of the breach (along the direction of flow through the breach). The flow scoured the breach and removed the bed sediments. On both sides of the breach wall, the instability and the collapse of the soils resulted in the continuing lateral widening of the breach. The inner river had dry wash at the initial moment. The flow then poured from the break into the inner river. Potential energy was rapidly transformed into kinetic energy. The greater the breach flow velocity was, the faster the breach expanded because of the strong scouring effects. As the water head in and out of the river and the breach lateral widening shrank, the flow velocity was gradually reduced. As shown in Fig. 7c and d, the velocity of breach lateral widening slowed down progressively.

Torrents of water flow were formed during the levee breaching process. Measuring the flow rate through the breach is difficult. Thus, a mathematical model was used to calculate the flow rate at the breach. As the breach expanded after flow overtopping, the flow rate through the breach increased, gradually reaching a peak value. The oscillation was

Table 1. Comparison of the computed with measured final breach width.

Levee material	Discharge ($L\,s^{-1}$)	Initial water head (cm)	Measured final breach width (cm)		Computed final breach width (cm)	
			Inner river	Outer river	Inner river	Outer river
Coarse sand	7.55	18	68	87	66.8	86.1
Coarse sand	13.22	18	75	96	76.3	96.6
Coarse sand	15.62	18	82	100	83.2	97.8
Coarse sand	6.55	15	55	86	56.5	83.6
Coarse sand	11.59	15	66	89	66.2	90.9
Coarse sand	15.04	15	74	98	75.1	96.4
Fine sand	7.28	18	62	90	62.8	91.0
Fine sand	11.57	18	73	98	72.2	99.3
Fine sand	15.08	18	86	110	88.5	112.6

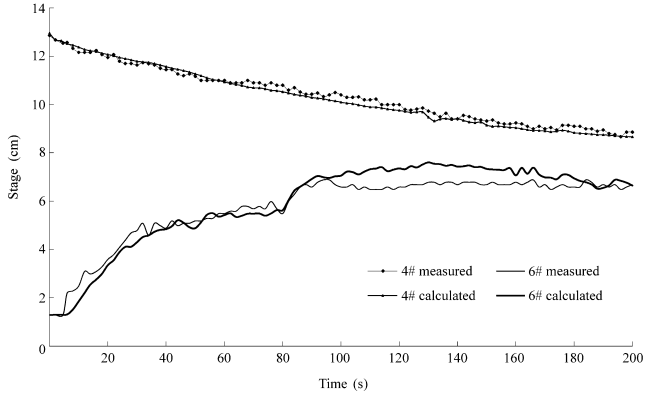

Fig. 6. Comparison between the calculated water level and actual water level.

reduced, and the flow rate finally stabilized. Owing to the straight flow and the one-sided break on the watercourse in this experiment, the discharge was mostly stabilized and over half of the total flow passed in the watercourse. Figure 8 shows that the water head in and out of the levee was 18 cm and 15 cm, respectively, when the total discharge at the inlet of the flume was $11.57\,L\,s^{-1}$. The flow rate through the breach is also shown in the figure. As shown in the figure, the discharge through the breach sharply increased after the levee breach. At about $t = 60$ s, the flow rate into the floodway district reached the peak value. When the water head in and out of the course was $h = 18$ cm, the peak flow rate through the breach was $6.97\,L\,s^{-1}$, accounting for 60.2 % of the total discharge. When $h = 15$ cm, the peak discharge through the breach was reduced to $6.01\,L\,s^{-1}$, accounting for 51.9 % of the total discharge. After reaching the peak discharge, the water head at both sides was gradually reduced, consequently reducing the discharge through the breach. The flow rate through the breach finally stabilized to 4.04 and $3.83\,L\,s^{-1}$. Most of the flows flowed downstream through the original watercourse.

3.3 Changing process of the breach

After flow overtopping, the levee top was quickly weakened by the effects of the flows, which initially formed rills. Soils at both sides gradually collapsed because of the lateral widening. The mouth development process in the burst is shown in Fig. 9.

Figure 10 shows the undercutting process through breach simulation. As shown in the figure, expansion of the incipient incision on the top of the levee was governed by a geotechnical failure as the slope was great; after that the sand is carried by flow. At about 20 s at the beginning of the levee breach, the breach crest level dropped drastically from 15 cm to approximately 8 cm. With the flow velocity getting smaller, the decreasing velocity of the breach crest level was significantly slowed down and stabilized at 4 cm. At the end of the experiment, the maximal height of the measured elevation was approximately 3.8 cm, which is generally consistent with the simulation results.

On the basis of the plane modality, the breach width on one side of the watercourse in the floodway district was wider than that on the other side. The top width of the breach on one side was larger than the bottom width, which can be attributed to the soil accumulation on the bottom of the breach after the suspension and collapse, consequently shrinking the bottom width of the breach. As the water level and the flow velocity stabilized, the breach width gradually stabilized. Erosion and deposition of sediments eventually reached a balance. Comparison between the actual stabilized breach width and the calculated stabilized breach width revealed that the maximal relative error between the two did not exceed 5 %, indicating the validity of the model adopted in this study, as it is shown in Table 1.

Figures 11 to 13 show the breach width changing process in the watercourse simulated in different conditions. As shown in the figures, the lateral widening did not start during the flow overtopping, but occurred after a period of time. The breach expansion velocity and the stabilized width were

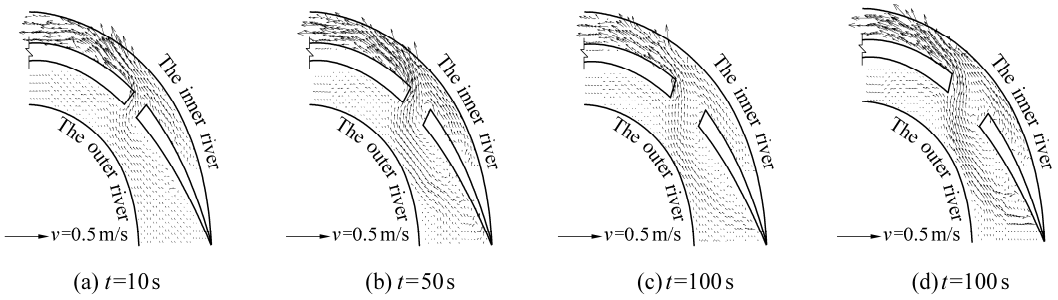

Fig. 7. Typical flow field near the breach.

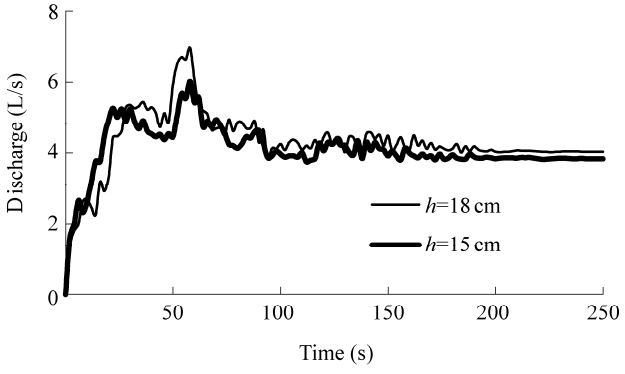

Fig. 8. Flow rate through the breach.

positively correlated with the total discharge Q in the watercourse. The levee body piled by coarse sediment particles was scoured by the flow and had smaller lateral widening velocity. Finally, no significant difference was observed between the stable breach width and the breach width of the levee piled by refined sediments. During the levee breach, the water head h at the breach at initial time determined the widening rate. The greater the h was, the greater was the velocity of lateral widening of the breach. Thus, a larger stable breach width can be finally formed.

4 Conclusions

In the paper, a mathematical model that can calculate the flow and sediment transport in levee breach was established. Based on hydrodynamics and morphodynamics, this model can accurately reflect the water level changing process on both sides of the watercourse after levee breaching by analyzing the flow velocity distribution, the scouring, and the widening of the breach and discharge. Experimental data on levee breaching proved the effectiveness of the algorithms used in the model and the processing patterns, indicating that the calculation mode adopted in this research can simulate the flow and sediment transport. In addition, the effects of the discharge, the water head in and out of the watercourse, and the material composition of the bank on the flow and sediment transport were analyzed.

The water level on one side of the watercourse dropped after the levee breach. The outer water level of the breach increased because the outer water was constrained by the walls of the flume. The two water levels gradually grew closer and eventually reached a steady state. However, the water flow process caused by levee breaching in the floodway district was not constrained by walls.

In the sandy soil levee breaching, an etched groove was formed on the top of the levee after flow overtopping. The part of the levee under water was drastically scoured by the flow, resulting in the vertical undercutting and lateral widening. Consequently, that part of the levee was fractured because of the suspension of the levee above the water level, resulting in lateral widening. The lateral widening of the levee was attributed to these two modes. The breach lateral widening of the soil levee was accurately simulated in the scouring-collapse lateral widening mode on the basis of the mechanic concepts such as flow sheer force and the shear strength of the soil body.

The flow rate through the breach was closely related to the water head on both sides of the river. Considering the other conditions the same, the final peak discharge through the breach was positively correlated with the water head in and out of the watercourse at the beginning of the levee breach. At the beginning of the levee breach, the water head in and out of the watercourse was relatively large, and the break rapidly expanded. At the same time, the flow rate through the breach sharply increased. As the water head on both sides gradually decreased, the breach expansion slowed down. The flow rate reached a peak value and then reduced gradually until no change in the water level on both sides was observed. The flow rate through the breach reached a stable value as well.

This study reveals that for the sandy-soil levee composed of nonuniform particles we can accurately predict all the variables that are concerned during levee breach based on mechanics. Instead of some assumptions applied in other research, the proposed calculation mode of breach lateral widening, in which the part of the levee under the water

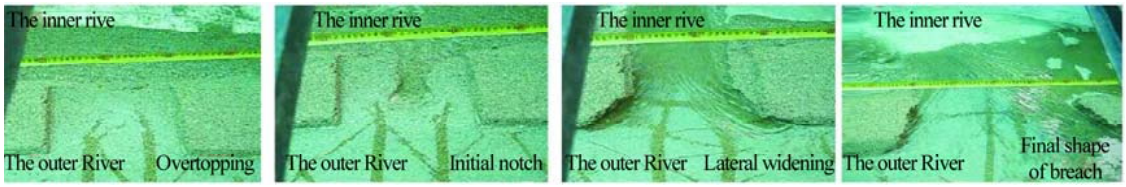

Fig. 9. Development of the levee breach.

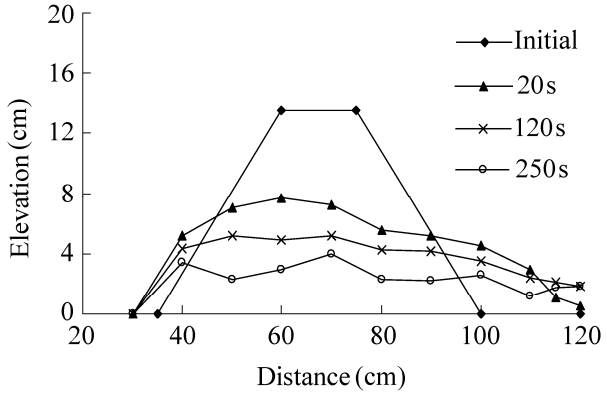

Fig. 10. Changing process of the breach cross-section along the flow.

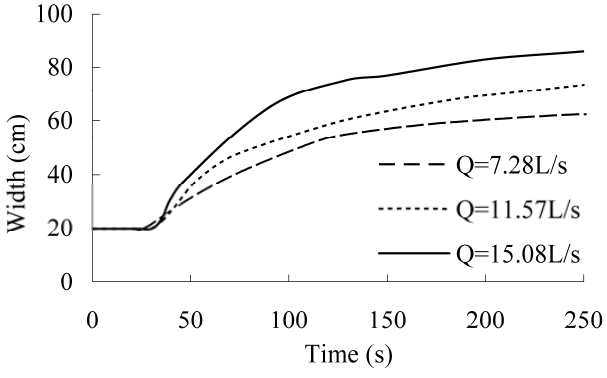

Fig. 11. Relationship between the break width changing process and the total discharge.

was subjected to lateral scouring, whereas the part above the water was subjected to the lateral widening from the suspending collapse, can effectively simulate the levee breach of sandy soil levee. The effectiveness of this model in practical levee breach calculation needs further verifications by using field data.

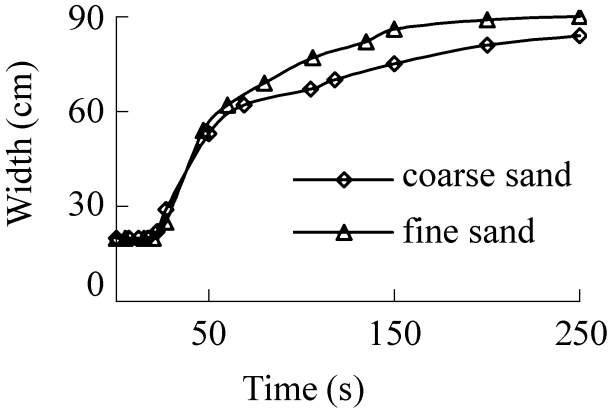

Fig. 12. Relationship between breach width and sediment grading.

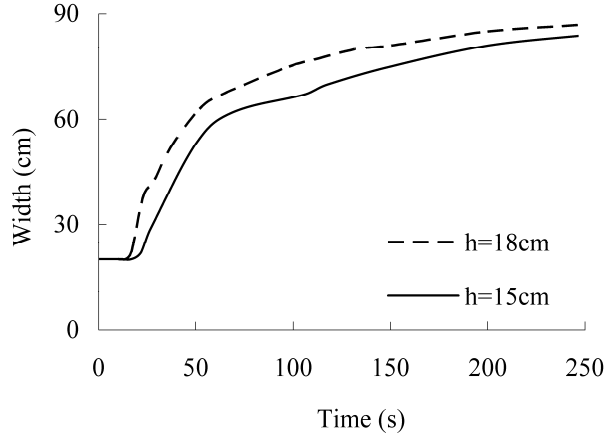

Fig. 13. Relationship between breach width and water head.

Acknowledgements. This study is supported by the National Basic Research Program of China (973 Program) and the National Natural Science Foundation of China (NSFC) under grant numbers 2011CB403306, 51209221, and 11272240, respectively.

Edited by: H. de Moel
Reviewed by: M. van Damme and one anonymous referee

References

Apel, H., Thieken, A. H., Merz, B., and Blöschl, G.: A probabilistic modelling system 5 for assessingflood risks, Nat. Hazards, 38, 79–100, 2006.

Chen, W. B., Liu, W. C., Wu, C. Y.: Coupling of a one-dimensional river routing model and a three-dimensional ocean model to predict overbank flows in a complex river–ocean system, Appl. Mathemat. Modell., 37, 6163–6176, 2013.

Cristofano, E. A.: Method of computing erosion rate for failure of earthfill dams. US Department of the Interior, Bureau of Reclamation, Engineering and Research Center, Washington DC, 1973.

Faeh, R.: Numerical Modeling of Breach Erosion of River Embankments, J. Hydraul. Engineer., 133, 1000–1009, 2007.

Fread, D. L.: DAMBRK: The NWS dam-break flood forecasting model, Vol. 4. Hydrologic Research Laboratory, National Weather Service, NOAA, Maryland, 1984

Fread, D. L.: BREACH, an erosion model for earthen dam failures, Hydrol. Res. Laborat., National Weather Service, NOAA, Maryland, 1988.

Harris, G. W. and Wagner, D. A.: Outflow from Breached Earth Dams. University of Utah, Salt Lake City, Utah. BSc. thesis, 1967.

Liu, W. C. and Wu, C. Y.: Flash flood routing modeling for leveebreaks and overbank flows due to typhoon events in a complicated river system, Nat. Hazards, 58, 1057–1076, 2011.

Lou, W. C.: Mathematical modelling of earth dam breaches. Colarado State University, Fort Collins, Colorado, USA, 1981.

Morris, M. W., Kortenhaus, A., and Visser, P. J.: Modelling breach initiation and growth, FLOODsite Report T06-08-02. FLOODsite, 2009.

Nogueira, V. A.: Mathematical Model of Progressive Earth Dam Failure, Colarado State University, Fort Collins, Colarado, USA, 1984.

Osman, A. M and Thorne, C. R.: Riverbank stability analysis I: Theory. ASCE, J. Hydraul. Engineer., 114, 134–150, 1988.

Roe, P. L.: Approximate Riemann solvers, parametervectors, and difference shemes, J. Computat. Phys., 43, 357–372, 1981.

Savant, G., Berger, C., McAlpin, T. O., and Tate, J. N.: Efficient implicit finite-element hydrodynamic model for dam and levee breach, J. Hydraul. Engineer., 137, 1005–1018, 2010.

Shu, C. W.: High-order finite difference and finite volume WENO schemes and discontinuous Galerkin methods for CFD, Internatl. J. Computat. Fluid Dynam., 17, 107–118, 2003.

Toro, E. F.: Shock-capturing methods for free-surface shallow follows. Chichester, New York, John Wiley, 2001.

Wang, D. W., Yang, G. L., Yu, M. H., Wang, M., and Dou, S. T.: A new semi-implicit scheme for two-dimensional convection equation, Engineering Journal of Wuhan University, 40, 18–21, 2007.

Wang, D. W., Liu, X. F., Chen, J. G., and Ji, Z.W.: The slop flux method for numerical balance in using Roe's approximate Riemann solver, J. Hydrodynam., 24, 58–64, 2012.

Wu, W. and Wang, S. S. Y.: One-dimensional modeling of dambreak flow over movable beds, J. Hydraul. Engineer., ASCE, 133, 48–58, 2007.

Wu, W., Marsooli, R., and He, Z.: Depth-Averaged Two-Dimensional Model of Unsteady Flow and Sediment Transport due to Noncohesive Embankment Break/Breaching, J. Hydraul. Engineer., ASCE, 138, 503–516, 2012.

Yu, M. H., Deng, Y. L., Qin, L. C., Wang, D. W, and Chen, Y. L.: Numerical simulation of levee breach flows under complex boundary conditions, J. Hydrodynam., 21, 633–639, 2009.